Catalysis Today 139 (2008) 202–208

Contents lists available at ScienceDirect

Catalysis Today

journal homepage: www.elsevier.com/locate/cattod

Sb–V–O-based catalysts for the ammoxidation of propane with a fluidized bed reactor

M. Olga Guerrero-Pérez [a,*], José L. Rivas-Cortés [a], J.A. Delgado-Oyagüe [a,1], J.L.G. Fierro [b], Miguel A. Bañares [b]

[a] Centro Tecnológico de Repsol-YPF, Autovía N-V Km 13, E-28931 Móstoles, Spain
[b] Instituto de Catálisis y Petroleoquímica (CSIC), Marie Curie 2, E-28049 Madrid, Spain

ARTICLE INFO

Article history:
Available online 2 September 2008

Keywords:
V–Sb–Al
V–Sb–Si
V–Sb–Nb–Si
V–Sb–O
Fluid bed
Ammoxidation
Propane
Acrylonitrile
Structure–activity relationship

ABSTRACT

Propane ammoxidation is usually investigated with fixed-bed reactors at laboratory scale; however, this kind of reactions takes place over fluid-bed reactors in industry. The present paper investigates the catalytic ammoxidation of propane over supported Sb–V–O catalysts using a fluidized bed microreactor. The effect of support, Sb/V atomic ratio, Sb + V total coverage, synthesis procedures, as well as the effect of Nb as additive of the Sb–V–O system were evaluated. The activity results show that the selectivity trends are quite similar to those obtained with a fixed-bed reactor but a higher amount of active phase is necessary for the fluidized bed catalysts to obtain similar acrylonitrile yields.

1. Introduction

The majority of the industrial organic products are manufactured with oil and natural gas. Nearly 25% of these compounds are prepared via selective oxidation and ammoxidation reactions using heterogeneous catalysts; so, paraffin selective ammoxidation to nitriles is a very important process to obtain organic products traditionally generated from petroleum [1–3]. Propane ammoxidation is especially important since it would be an alternative to the actual propylene ammoxidation. Thus, in 1997 British petroleum (bp) started a demonstration plant to make acrylonitrile, using propane, and estimated to decrease production costs ca. 20% compared with conventional propylene-based technology [4].

There are several studies about catalysts used for propane ammoxidation, but the major part of the reported work is concentrated on two types of catalysts [1–3], the antimonates with rutile structure [5–11] and the molybdates [12–15], both systems usually incorporate vanadium as the key element. Alumina has been described as a good support of this system and there are several patents with synthesis procedures for the Al–Sb–V–O system [16], the selectivity to acrylonitrile and propylene was found to be higher on catalysts supported on alumina than on unsupported, especially for higher conversions [17]. Previous results with a micro-fixed-bed reactor, showed a good performance of supported Sb–V–O catalysts [18,19]; and it was found that the support determines both structure and catalytic behavior of catalysts [20].

The fixed-bed reactor is widely used due to the simple technology that it requires; under certain premises, fluidized bed reactors are necessary. Pressure built-up can be quite important for large reactor lengths and reactants fluxes. In practice, the pressure increase becomes the factor that determines the smallest particle diameter that can be used. Larger particles present internal diffusional resistance, so, they cannot be used [21]. Processes with a high rate of heat exchange, e.g. strongly exothermic reactions, pose serious limitation on the temperature control in a fixed-bed reactor, which can result in catalyst or reactor damage. Uncontrolled temperature increase may decrease selectivity values; which is the case for the oxidation and ammoxidation of propane. Industrially, propane ammoxidation would only take place in a fluid-bed reactor; yet only a few works report fluidized Sb–V–O catalysts [22,23].

Sb–V–O and Sb–V–Nb–O fluid-bed catalysts supported on Al_2O_3 and SiO_2 are studied in present paper. Catalysts were prepared

* Corresponding author at: Departamento de Ingeniería Química, Facultad de Ciencias, Universidad de Málaga, Campus de Teatinos, E-29071 Málaga, Spain. Tel.: +34 95 213 1378.
E-mail address: oguerrero@uma.es (M.O. Guerrero-Pérez).
[1] Deceased.

0920-5861/$ – see front matter © 2008 Elsevier B.V. All rights reserved.
doi:10.1016/j.cattod.2008.07.021

according to two different synthesis methods, the standard, in which antimony is added as a Sb_2O_3 suspension, and a new method in which antimony is added as soluble tartrate complex [24,25]. This paper evaluates the role of the support, the synthesis method and the role of Nb as an additive on supported Sb–V–O catalysts. The results are compared with those previously reported with a conventional fixed-bed reactor.

2. Experimental and methods

2.1. Preparation of samples

Two series of catalysts are prepared, the (Nb)–Sb–V/support-(Sb_2O_3) and the Nb–Sb–V/support-(SbT) series, which use Sb_2O_3 suspension (slurry) or a molecularly dissolved Sb precursor (tartrate). The (Nb)–Sb–V/support-(Sb_2O_3) catalyst series was prepared by a slurry method. Sb_2O_3 (Aldrich, p.a.) was added to an aqueous solution of NH_4VO_3 (Sigma, p.a.) and an ammonium niobium soluble complex (Niobium Products), heating and stirring at 80 °C for 50 min, then, γ-Al_2O_3 (Versal, 265 m^2/g) or SiO_2 (XPO 2407, Grace Division) was added. The resulting solution was dried in a rotavapor at 80 °C. The resulting solid was dried at 115 °C for 24 h and then was calcined in air at 400 °C for 4 h. The Nb–Sb–V/support-(SbT) catalysts were prepared dissolving the necessary quantity of antimony acetate (Aldrich) on tartaric acid (Sigma) 0.3 M [24,25]. This solution was kept under stirring until all antimony was dissolved. Then, NH_4VO_3 (Sigma), ammonium niobium soluble complex (Niobium Products) and γ-Al_2O_3 or SiO_2 were added. The resulting solution was dried in a rotavapor at 80 °C. The resulting solid was dried at 115 °C for 24 h and then was calcined in air at 400 °C for 4 h.

The catalysts were prepared so that a total coverage of V + Sb or V + Sb + Nb would correspond to the dispersion limit or four times this value on the corresponding support (i.e., total of 9 atoms/nm^2 of support on alumina or total of 1 atom/nm^2 of support on silica). The dispersion limit was determined by Raman spectroscopy in a VO_x/Al_2O_3 series, as the maximum surface loading of VO_x units that remain dispersed, with no crystalline V_2O_5 (at V/nm^2) [26]. The Sb/V and Sb/V atomic ratio changed in the one to three intervals for de Sb/V and was fixed to one for the Nb/Sb ratio.

2.2. Characterization

Nitrogen adsorption isotherms (−196 °C) were recorded on an automatic Micromeritics ASAP-2000 apparatus. Prior to the adsorption experiments, samples were outgassed at 413 K for 2 h. BET areas were computed from the adsorption isotherms ($0.05 < P/P_0 < 0.27$), taking a value of 0.164 nm^2 for the cross-section of the adsorbed N_2 molecule at −196 °C. X-ray diffraction patterns were recorded on a Siemens Krystalloflex D-500 diffractometer using Cu Kα radiation ($\alpha = 0.15418$ nm) and a graphite monochromator. Working conditions were 40 kV, 30 mA, and scanning rate of 2°/min for Bragg's angles (2θ) from 5° to 70°. In some cases, the peaks of Al from the sample holder are present.

The particle size distribution was determined with a Mastersizer apparatus (Malvern). It has been used laser light dispersion in small angle, commonly called laser diffraction. The sample is like a powder and is pushed with air with a pressure of 2 bar. The apparatus uses a laser of He–Ne.

Raman spectra were run with a single-monochromator Renishaw System 1000 equipped with a cooled CCD detector (200 K) and holographic Notch filters. The holographic Notch filters remove the elastic scattering. The samples were excited with the 514 nm Ar line; spectral resolution was ca. 3 cm^{-1} and spectrum acquisition consisted of 10 accumulations of 30 s. The spectra were obtained under dehydrated conditions (ca. 390 K) in a hot stage (Linkam TS-1500). Hydrated samples were obtained at room temperature after and under exposure to a stream of humid synthetic air. Silica-supported catalysts could not be characterized by Raman spectroscopy due to an overwhelming fluorescence background.

2.3. Activity measurements

Activity measurements were performed using a microplant with feed lines for air, nitrogen and ammonia. The fluid-bed reactor is made of quartz, it has a porous plate in the base that distributes the flux and then it has two porous plates to achieve a good fluidization. It has an internal tube for the thermocouple. At the end of the reactor there is an expansion camera. A glass carcass protects the reactor. External resistances that heat the system surround it and permit to see the interior of the reactor during reaction. CO, CO_2, ethylene, oxygen, nitrogen, propylene and propane are analyzed on line with a 5890 Hewlett Packard gas chromatograph. The CG also has a FID detector for the analysis of acrylonitrile, acrolein and acetonitrile that are recovered in absorbed lunges with HCl; in this case, the sample is injected with an automatic injector. NH_3 and HCN were determined by titration methods. Yields and selectivities in products were determined on the basis of the moles of propane feed and products, considering the number of carbon atoms in each molecule. The correctness of the analytical determinations was checked for each test by verification that the carbon balance (based on the propane converted) was within the cumulative mean error of the determinations (±10%). Tests were made using the following feedstock: 9.8% propane, 8.6% ammonia and the rest air. The total flow rate was 20 N L h^{-1} and 40 g of catalysts were used. Such parameters were experimentally determined to reach a good fluidization regime [27]. Temperature reaction was 450 °C. To verify the reliability of our micro-fluid-bed reactor, a test of propylene ammoxidation with a commercial catalyst was made. 90% propylene conversion was obtained at 430 °C and selectivity to acrylonitrile was higher than 70%.

3. Results and discussion

3.1. Alumina-supported catalysts

Table 1 shows the BET surface areas, the composition obtained by ICP, the Sb/V molar ratios and the Sb + V total coverage values. The BET area values for the Sb–V catalysts decrease when the surface coverage increases. The atomic Sb/V ratios do not appear to have a clear effect on BET area values. Catalysts prepared with tartaric acid present higher BET area values. Fig. 1 shows the granulometric distributions for Sb–V–O/Al catalysts. The distribution shows a maximum near 100 μm and another small maximum

Table 1
Composition determined by ICP and BET area of alumina-supported Sb–V–O catalysts

Catalyst	Sb + V total coverage	Sb/V molar ratio	%Sb	%V	BET area (m^2/g)
1Sb1V/Al–(SbT)	1	1	5.2	12.4	177
1Sb3V/Al–(SbT)	1	3	2.4	17.0	130
4Sb1V/Al–(SbT)	4	1	9.1	21.8	71
4Sb3V/Al–(SbT)	4	3	3.9	28.2	58
1Sb1V/Al–(Sb_2O_3)	1	1	6.1	14.7	138
1Sb3V/Al–(Sb_2O_3)	1	3	3.0	21.6	125
4Sb1V/Al–(Sb_2O_3)	4	1	12.6	30.1	67
4Sb3V/Al–(Sb_2O_3)	4	3	6.1	43.5	36

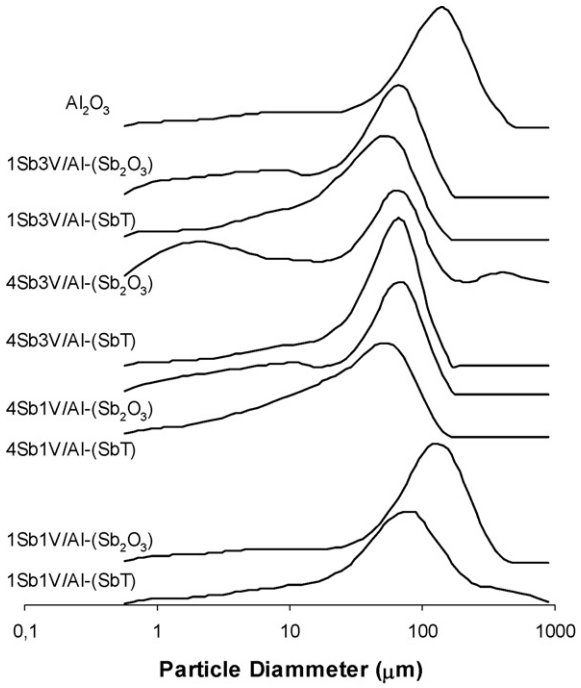

Fig. 1. Granulometric distributions of alumina-supported Sb–V–O catalysts.

near 10 μm (fines) for the catalysts prepared with Sb_2O_3 suspension. This fact makes their average particle lower than in the case of tartrate-series, although the main maximum appears at higher particle diameter values for catalysts prepared with Sb_2O_3. The lower presence of fines in the case of samples prepared with tartrate make these catalysts more convenient for the fluidized bed reactor.

The XRD patterns of fresh and used alumina-supported catalysts are shown in Fig. 2. Catalysts that present diffraction pattern of $VSbO_4$ phase before reaction are those prepared with the tartrate method and with high coverage (Sb + V = 4), thus, the tartrate method enhances the formation of the mixed Sb–V–O phase during synthesis. After reaction the pattern of $VSbO_4$ becomes also evident for $4Sb_1V/Al–(Sb_2O_3)$, indicating that $VSbO_4$ formation is favored during propane ammoxidation.

The catalysts prepared with the tartrate method do not exhibit the diffraction patterns of antimony oxides, in agreement with previous studies [24,25]. Fresh and used catalysts prepared with Sb_2O_3 at coverages of one monolayer generate the diffraction pattern of Sb_2O_3 and α-Sb_2O_4 phases. The intensity for the α-Sb_2O_4 peaks with respect those of Sb_2O_3 is higher in the aged samples; however, Sb_2O_3 phase still remains present in the used samples. On the contrary, no Sb_2O_3 diffraction pattern is observed for used catalysts with four monolayers. It has been proposed a catalytic cycle in which V^{5+} species dispersed on the surface of catalysts combine with Sb species to form $VSbO_4$ and Sb_2O_4 during propane ammoxidation in a fixed-bed reactor [28,29]. XRD data do not show such a transformation, which may be indicative that the rutile $VSbO_4$ phase domains may be nanoscaled and not large enough to generate X-ray diffraction pattern. Such a phase is apparent in catalyst used in a fixed-bed reactor. It appears that both, ammoxidation reaction and reconstruction of supported V and Sb species into the $VSbO_4$ phase is more favorable in a fixed-bed reactor [28,29]; probably due to higher contact times.

Fig. 3 shows the Raman spectra of fresh and used dehydrated alumina-supported catalysts. Reference Sb_2O_3 exhibits Raman bands at 190, 255, 372, 451 and 716 cm^{-1} (not shown), α-Sb_2O_4 shows Raman bands at 190, 261, 399 and 459 cm^{-1} (not shown), and V_2O_5 shows Raman bands at 143, 283, 302, 405, 480, 526, 698 and 994 cm^{-1} (not shown) [18]. A broad Raman band near 800 cm^{-1} that corresponds to the rutile $VSbO_4$ phase [30], is present in catalyst $1Sb_3V/Al–(Sb_2O_3)$, and in fresh and used samples with Sb + V = 4. Thus, both XRD and Raman evidence that the tartrate method and the excess of Sb enhances $VSbO_4$ formation during synthesis. $VSbO_4$ aggregates must be small in $1Sb_3V/Al–(Sb_2O_3)$ since its diffraction pattern is not evident. The broad Raman band appears be constituted by two Raman bands at 835 and 795 cm^{-1}, which are well resolved by UV-Raman spectroscopy [30,31]. These bands shift to higher Raman shifts for $1Sb_3V/Al–(SbT)$, $1Sb_1V/Al–(SbT)$ and $4Sb_1V/Al–(SbT)$. This shift is related to the presence of a component near 888 cm^{-1},

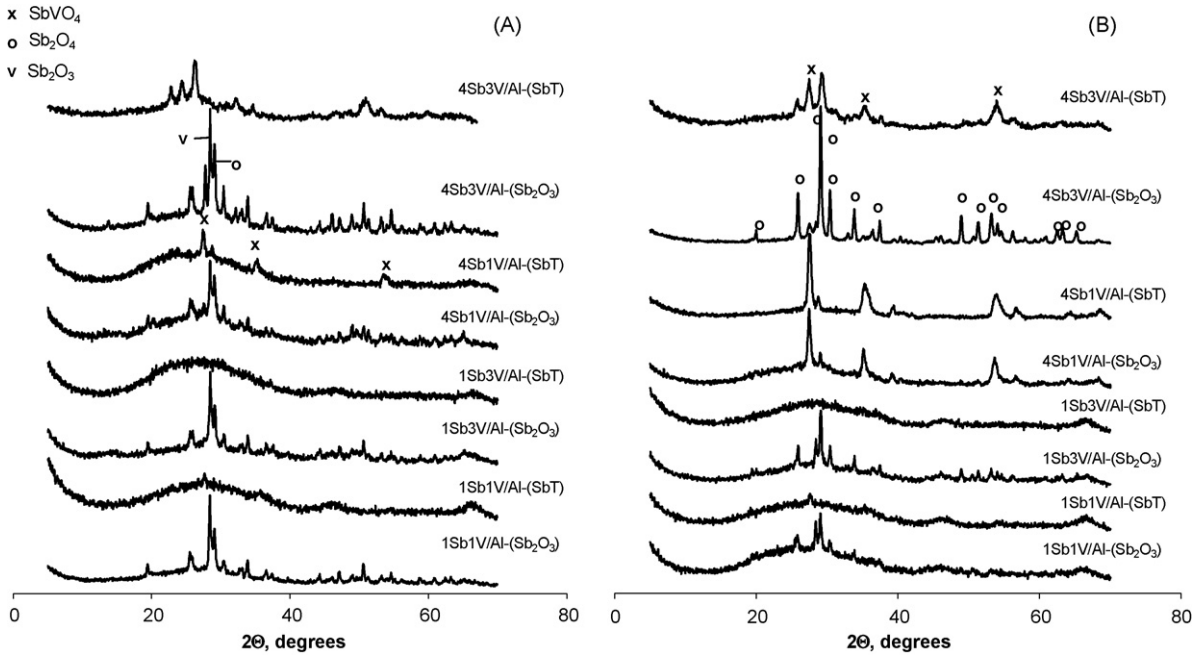

Fig. 2. XRD patterns of fresh (A) and used (B) alumina-supported Sb–V–O catalysts.

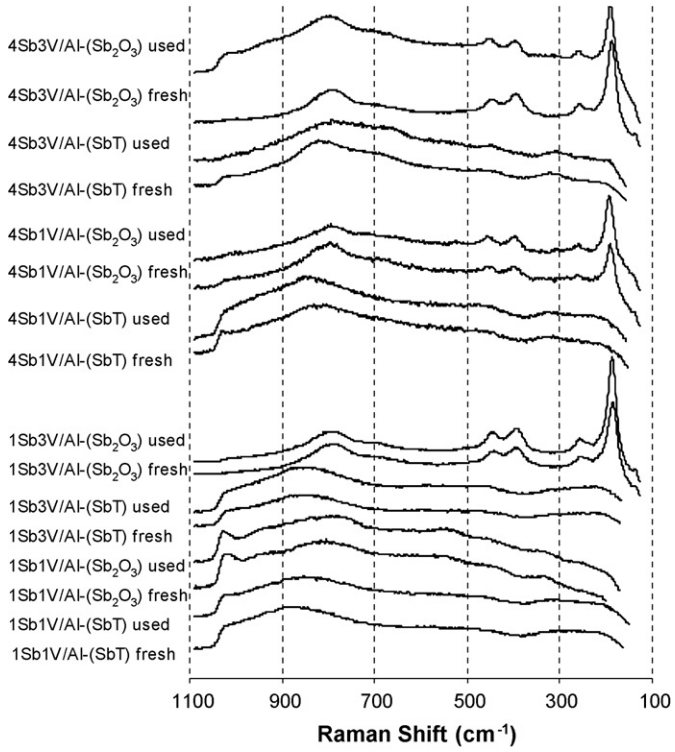

Fig. 3. Dehydrated in situ Raman spectra of fresh and used alumina-supported Sb–V–O catalysts.

characteristic of surface defects at the surface of the rutile $VSbO_4$ phase [30,31]. In general, molecularly dissolved antimony (tartrate) blends more efficiently with vanadium sites than when a suspension on Sb_2O_3 particles is used [30], which results in a more intense Raman band of the surface defects. Thus, tartrate method induces the presence of Sb vacancies in the rutile $VSbO_4$ phase. The Raman band near 1024 cm^{-1}, sensitive to hydration that is present in fresh and used catalysts prepared with tartaric acid, belongs to the V=O stretching mode of surface VO_x species [32]. These vanadium species are involved in the activation of propane molecule since vanadium alkoxides are detected during reaction [28,29].

Table 2 shows the catalytic performance of alumina-supported Sb–V–O catalysts. Acrylonitrile yields are lower in the fluid-bed reactor than in the fixed-bed reactor. This is in part due to the high CO_x selectivity in the fluid-bed reactor, related with larger void volume compared to fixed-bed reactor. Similar results were achieved by Massetti et al. [22]. The catalysts prepared by the tartrate method afford higher selectivities towards propylene and acrylonitrile.

The more active catalysts (Table 2) are obtained when total Sb + V coverage is one monolayer. At higher coverages the interaction between Sb and V is more favored, which maximizes the number of vanadium sites that combine with antimony. So, catalysts with one monolayer and Sb/V = 1 atomic ratio present vanadium VO_x species (Raman spectra in Fig. 3); which activate propane. This renders the system active, yet selectivity is low, since the CO_x dominates product distribution, being the selectivity to acrylonitrile low.

3.2. Silica-supported catalysts

The BET areas of the silica catalyst are listed in Table 3. The BET area values for the Sb–V oxide catalysts decrease with surface coverage of Sb + V. The preparation method, atomic Sb/V ratio and Sb/Nb ratios do not appear to have a clear effect on BET area values.

Fig. 4 shows the granulometric distributions for Sb–V–O/Si and Sb–V–Nb–O/Si catalysts. There is a decrease in the population of fines, compared to that obtained for the alumina-series. This makes silica-supported catalysts more adequate for their use in the

Table 2
Catalytic performance of alumina-supported Sb–V–O catalysts

Catalyst	C_3H_8 conversion (%)	CO_2 selectivity (%)	CO selectivity (%)	Propylene selectivity (%)	Acetonitrile selectivity (%)	Acrylonitrile selectivity (%)
1Sb1V/Al–(SbT)	61.8	41.0	37.5	13.5	1.7	7.2
1Sb3V/Al–(SbT)	41.0	50.7	18.5	17.1	1.4	12.3
4Sb1V/Al–(SbT)	50.9	51.0	23.1	20.8	1.3	3.8
4Sb3V/Al–(SbT)	48.5	4.0	40.8	43.5	1.3	10.8
1Sb1V/Al–(Sb_2O_3)	65.3	24.1	62.2	11.2	1.1	1.4
1Sb3V/Al–(Sb_2O_3)	48.7	3.1	74.5	21.2	0.4	0.8
4Sb1V/Al–(Sb_2O_3)	48.9	52.0	24.1	21.8	0.36	1.8
4Sb3V/Al–(Sb_2O_3)	55.5	14.0	40.5	43.5	1.3	0.7

Reaction conditions: total flow 20 N L h^{-1}, 400 mg of catalyst; temperature: 450 °C; feed composition (% volume): 9.8% propane, 8.6% ammonia and the rest air.

Table 3
Composition determined by ICP and BET area of silica-supported Sb–V–O catalysts.

Catalyst	Sb + V total coverage	Sb/V molar ratio	Sb/Nb molar ratio	%Sb	%V	% Nb	BET area (m^2/g)
1Sb1V/Si–(SbT)	1	1	–	2.5	1.0	–	214
1Sb3V/Si–(SbT)	1	3	–	3.7	0.5	–	228
4Sb1V/Si–(SbT)	4	1	–	7.9	3.3	–	192
4Sb3V/Si–(SbT)	4	3	–	11.3	1.7	–	169
1Sb1V/Si–(Sb_2O_3)	1	1	–	2.6	1.1	–	216
1Sb3V/Si–(Sb_2O_3)	1	3	–	3.8	0.6	–	235
4Sb1V/Si–(Sb_2O_3)	4	1	–	8.8	3.7	–	188
4Sb3V/Si–(Sb_2O_3)	4	3	–	13.0	1.8	–	177
4Sb1V1Nb1/Si–(Sb_2O_3)	4	1	1	5.9	2.4	4.5	187
4Sb1V1Nb1/Si–(SbT)	4	1	1	5.4	2.3	4.2	193
4Sb3V1Nb1/Si–(Sb_2O_3)	4	3	1	10.4	1.7	2.6	205
4Sb3V1Nb1/Si–(SbT)	4	3	1	8.9	1.4	2.4	188

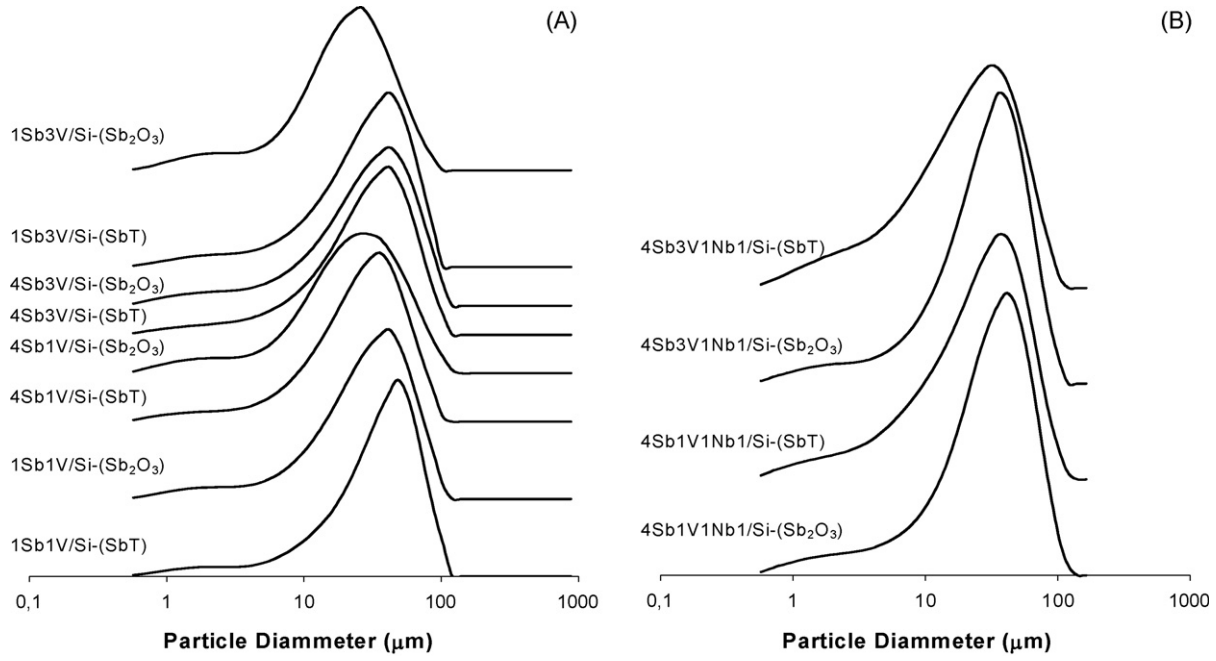

Fig. 4. Granulometric distributions of silica-supported Sb–V–O catalysts (A) and Sb–V–Nb–O catalysts (B).

fluidized bed reactor. The distributions obtained with the tartrate method are narrower than with the standard method.

Fig. 5A shows the XRD patterns of fresh and used Sb–V silica-supported catalysts with Sb + V total coverage of four monolayers. The XRD patterns of catalysts with coverage of one monolayer are not shown since no diffraction pattern is observed; thus indicating that oxide phases are essentially dispersed on silica support or the size of the aggregates is not larger than 4 nm. $VSbO_4$ pattern is visible in fresh catalysts prepared with tartrate (Fig. 5A); again, as in the alumina-series, tartrate method maximizes Sb–V oxides interaction leading to rutile $VSbO_4$ phase formation. In line with alumina-series, propane ammoxidation affects the structure of the catalyst. Thus, $VSbO_4$ diffraction pattern is evident in aged $4Sb_1V/Si–(Sb_2O_3)$ sample. Catalysts with Sb/V = 3 that possess Sb_2O_3 and Sb_2O_4 oxides, increase the Sb_2O_4/Sb_2O_3 after use in propane ammoxidation.

Fig. 5B shows the XRD patterns of the niobium-doped series. The rutile $VSbO_4$ diffraction pattern is not present in any fresh samples and it is only present in used catalysts, when they are prepared via the tartrate method and at an atomic Sb/V = 1 atomic

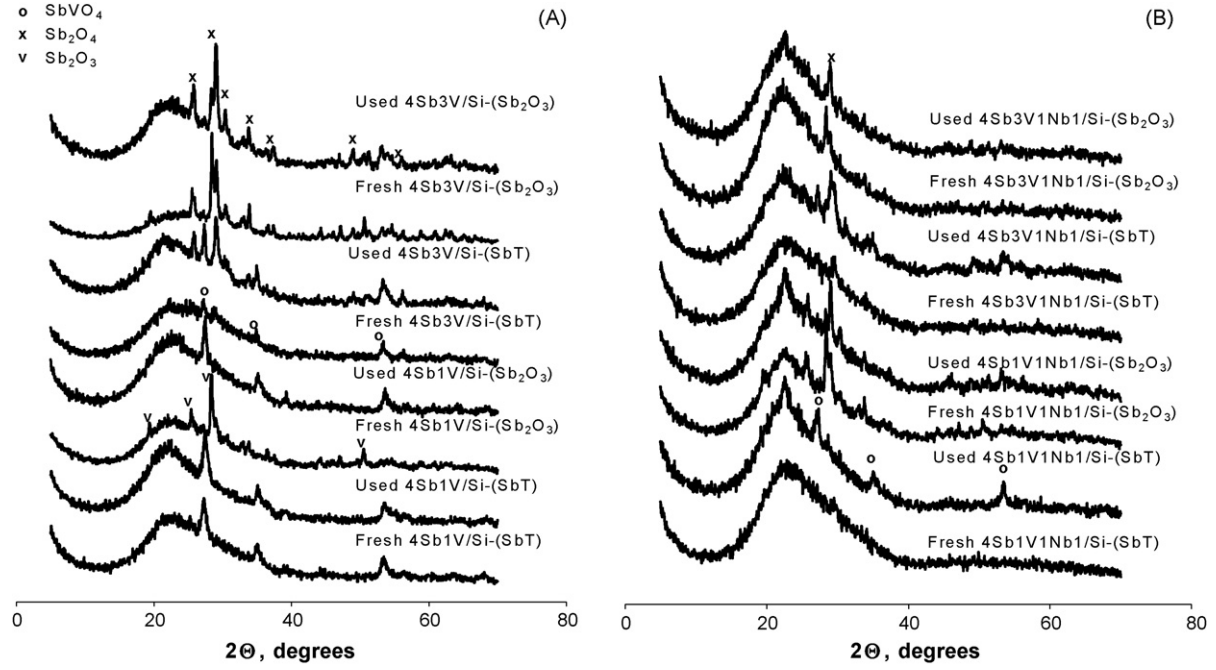

Fig. 5. XRD patterns of fresh and used silica-supported Sb–V–O catalysts (A) and Sb–V–Nb–O catalysts (B).

Table 4
Catalytic performance of silica-supported Sb–V–O catalysts

Catalyst	C_3H_8 conversion (%)	CO_2 selectivity (%)	CO selectivity (%)	Propylene selectivity (%)	Acetonitrile selectivity (%)	Acrylonitrile selectivity (%)
1Sb1V/Si–(SbT)	34.3	4.0	37.6	50.6	0.9	6.9
1Sb3V/Si–(SbT)	17.1	1.0	18.8	79.5	0.2	0.5
4Sb1V/Si–(SbT)	52.1	38.4	37.5	23.8	0.0	0.3
4Sb3V/Si–(SbT)	25.7	11.4	41.8	38.3	0.9	7.6
1Sb1V/Si–(Sb_2O_3)	35.2	4.0	36.7	53.1	0.8	5.3
1Sb3V/Si–(Sb_2O_3)	8.5	3.4	8.2	86.2	1.0	0.9
4Sb1V/Si–(Sb_2O_3)	43.6	4.6	60.0	34.4	0.2	0.8
4Sb3V/Si–(Sb_2O_3)	17.8	2.5	30.1	61.0	0.8	5.6

Reaction conditions: total flow 20 N L h^{-1}, 400 mg of catalyst; temperature: 450 °C; feed composition (% volume): 9.8% propane, 8.6% ammonia and the rest air.

Table 5
Catalytic performance of silica-supported Sb–V–Nb–O catalysts

Catalyst	C_3H_8 conversion (%)	CO_2 selectivity (%)	CO selectivity (%)	Propylene selectivity (%)	Acetonitrile selectivity (%)	Acrylonitrile selectivity (%)
4Sb1V1Nb1/Si–(Sb_2O_3)	16.4	2.4	28.5	61.7	0.8	6.6
4Sb1V1Nb1/Si–(SbT)	47.1	41.0	33.6	18.5	0.2	6.7
4Sb3V1Nb1/Si–(Sb_2O_3)	45.0	33.0	39.1	26.9	0.1	0.9
4Sb3V1Nb1/Si–(SbT)	30.0	5.1	47.2	39.2	0.5	8.1

Reaction conditions: total flow 20 N L h^{-1}, 400 mg of catalyst; temperature: 450 °C; feed composition (% volume): 9.8% propane, 8.6% ammonia and the rest air.

ratio ($4Sb_1V_1Nb_1$/Si–(SbT) catalyst). The XRD patterns of catalysts $4Sb_1V_1Nb1$/Si–(Sb_2O_3) and $4Sb_3VNb_1$/Si–(Sb_2O_3) show diffraction pattern of both Sb_2O_3 and Sb_2O_4, while only the diffraction pattern of Sb_2O_4 phase is observed in the used samples. The presence of Sb_2O_4 pattern in the used samples is consistent with the structural transformation in the Sb–V–O system during ammoxidation reaction [29].

Table 4 shows the activity results obtained with silica-supported Sb–V–O catalysts and Table 5 shows the catalytic performance of the Sb–V–Nb–O silica-supported catalysts. Propane conversion increases with vanadium content for Sb–V–O catalysts, suggesting that dispersed vanadium species are involved in the activation of the propane molecule, but such species must be less available when Nb is added, indicative of a possible Nb–V interaction [33]. Activity increases with coverage, a difference to that observed for the alumina-supported catalysts. As in the case of alumina series, the highest acrylonitrile selectivities are achieved with Sb + V = 4 and Sb/V = 3 regardless of the preparation method.

4. Conclusions

For a given catalyst, the fluidized bed reactor affords lower acrylonitrile yield than the fixed-bed reactor. The nature of the active site, which forms during propane ammoxidation, is the same regardless of the reactor configuration; however, V–Sb interaction is much lower in the fixed-bed reactor. The ammoxidation catalytic cycle blends V and Sb, and due to a different gas regime, the catalyst surface would have a different temperature profile, which would show on the solid-state reaction between vanadium and antimony. In addition, the higher space velocities could then limit total ammoxidation rates and the formation of $VSbO_4$ phase.

The novel synthesis method using tartaric acid is more convenient to prepare catalysts for fluidized bed reactors because it minimizes the finest particles. Furthermore, the particle distribution is narrower when the tartrate method is used. In addition, the tartrate method favors the formation of $VSbO_4$ active phase during synthesis and have been demonstrated that the catalytic cycle for acrylonitrile formation is more favored for catalysts prepared with the tartrate method.

Acknowledgements

This research was funded by Spanish Ministerio de Educación y Ciencia (grant CTQ2005-02802/PPQ) and COST Action D36/006/06, MOPG thanks the CSIC for an I3PDR-8-02 postdoctoral fellowship. The authors thank Dr. M.A. Vicente, from Salamanca University (Spain), for the XRD measurements and his helpful comments.

References

[1] R.K. Grasselli, in: Ertl., et al. (Eds.), Handbook in Catalysis, vol. V, Wiley–VCH, 1997 , p. 2302.
[2] R.K. Grasselli, Top. Catal. 23 (2003) 5.
[3] M. Bowker, C.R. Bicknell, P. Kerwin, Appl. Catal. A 136 (2) (1996) 205.
[4] Chemical Week, June 4, 1997, p. 5
[5] R. Catani, G. Centi, F. Trifirò, R.K. Grasselli, Ind. Eng. Chem. Res. 31 (1992) 107.
[6] G. Centi, F. Marchi, S. Perathoner, Appl. Catal. A 149 (1997) 225.
[7] G. Centi, P. Mazzoli, Catal. Today 28 (1996) 351.
[8] H.W. Zanthoff, W. Grünert, S. Buchholzs, M. Heber, L. Stievano, F.E. Wagner, G. Wolf, J. Mol. Catal. 162 (2000) 443.
[9] H.W. Zanthoff, S. Shafer, G.U. Wolf, Appl. Catal. A 164 (1997) 105.
[10] Y.C. Kim, W. Ueda, Y. Morooka, Catal. Today 13 (1992) 673.
[11] M.O. Guerrero-Pérez, M.V. Martínez-Huerta, J.L.G. Fierro, M.A. Bañares, Appl. Catal. A 298 (2006) 1, doi:10.1016/j.apcata.2005.09.013.
[12] S.I. Woo, J.S. Kim, Stud. Surf. Sci. Catal. 92 (1995) 191.
[13] J.S. Kim, S.I. Woo, Appl. Catal. A 110 (1994) 207.
[14] T. Ushikubo, K. Oshima, A. Kayou, M. Vaarkamp, M. Hatano, J. Catal. 169 (1997) 394.
[15] M.O. Guerrero-Pérez, J.N. Al-Saeedi, V. Vadim, M.A. Guliants, Bañares, Appl. Catal. A 260 (1) (2004) 93.
[16] US Patents 4,746,641 (1988); US Patents 4,784,979 (1988); US Patents 4,788,317 (1988); US Patents 4,871,706 (1989); US Patents 4,877,764 (1989); US Patents 4,879,264 (1989); assigned to the Standard Oil Company (OH).
[17] A. Andersson, S.L.T. Andersson, G. Centi, R.K. Grasselli, M. Sanati, F. Trifiro, Appl. Catal. A 113 (1994) 43.
[18] M.O. Guerrero-Pérez, J.L.G. Fierro, M.A. Vicente, M.A. Bañares, J. Catal. 206 (2002) 339, doi:10.1006/jcat.2001.3494.
[19] M.O. Guerrero-Pérez, J.L.G. Fierro, M.A. Bañares, Phys. Chem. Chem. Phys. 5 (2003) 4032, doi:10.1039/b307030a.
[20] M.O. Guerrero-Pérez, J.L.G. Fierro, M.A. Bañares, Catal. Today 78 (2003) 387, doi:10.1016/S0920-5861(02)00304-8.
[21] J.M. Santamaría, J. Herguido, M.A. Menendez, A. Monzón, "Ingeniería de Reactores" Editorial Síntesis, Madrid, 1999.
[22] S. Masetti, F. Trifirò, G. Blanchard, Appl. Catal. A 217 (2001) 119.
[23] A.H. Fakeeha, M.A. Soliman, A.A. Ibrahim, Chem. Eng. Process. 39 (2000) 161.
[24] M.O. Guerrero-Pérez, M.A. Bañares, Catal. Today 96 (2004) 265, doi:10.1006/j.cattod.2004.06.150.
[25] M.O. Guerrero-Pérez, J.L.G. Fierro, M.A. Bañares, Top. Catal. 41 (2006) 43, doi:10.1007/s11244-006-0093-7.
[26] I.E. Wachs, L.E. Briad, J.-M. Jehng, L. Burcham, X. Gao, Catal. Today 57 (2000) 323.

[27] M.O. Guerrero-Pérez, Ph.D. Dissertation, Universidad Autónoma de Madrid, Spain, 2003.
[28] M.O. Guerrero-Pérez, M.A. Bañares, Chem. Commun. (2002) 1292, doi:10.1039/b202556f.
[29] M.O. Guerrero-Pérez, M.A. Bañares, J. Phys. Chem. C 111 (2007) 1315, doi:10.1021/ie0510.
[30] M.O. Guerrero-Pérez, J.L.G. Fierro, M.A. Vicente, M.A. Bañares, Chem. Mater. 19 (2007) 6621, doi:10.1021/cm702022d.
[31] G. Xiong, V.S. Sullivan, P.C. Stair, G.W. Zajac, S.S. Trail, J.A. Kaduk, J.T. Golab, J.F. Brazdil, J. Catal. 230 (2005) 317.
[32] M.A. Bañares, .E. Wachs, J. Raman Spectrosc. 33 (2002) 359.
[33] M.O. Guerrero-Pérez, J.L.G. Fierro, M.A. Bañares, Catal. Today 118 (2006) 366.